Oxygen transport and exchange in oxide ceramics

B.C.H. Steele
Centre for Technical Ceramics, Department of Materials, Imperial College, London SW7 2BP (UK)

Abstract

Oxygen transport in most oxide ceramics incorporated in solid oxide fuel cells (SOFC) involves the movement of oxygen ion vacancies. It is the relative magnitude of oxygen ion vacancy and electronic charge carrier concentrations and mobilities which determines whether oxide materials can function as effective electrolyte or electrode components. Examination of relevant data suggests that zirconia- and ceria-based electrolytes are unlikely to be replaced in SOFC systems operating in the temperature range 450–950 °C. Oxygen ion vacancies are also involved in the cathodic reduction of oxygen and influence the magnitude of the associated exchange current density which can be measured by isotopic oxygen exchange measurements. Oxygen vacancy concentrations are also implicated in thermal expansion coefficient values and chemical stability considerations. It follows that optimisation of the cathode composition requires many conflicting requirements to be satisfied. However for operation at 800 °C, electrolyte, electrode and bipolar plate materials are available to ensure power densities approaching 0.5 W cm^{-2}. In contrast, direct methanol SOFC systems operating at 500 °C necessitate the development of alternative electrode materials. The successful exploitation of our knowledge about oxygen ion vacancy transport in ceramic oxides has now stimulated research into the role of protons in oxide lattices, and it is postulated that protonic/hydroxyl ion transport could be important in the development of alternative anode components.

1. Introduction

1.1. General

Ceramic fuel cells incorporating solid oxygen ion conducting electrolytes possess several advantages over other types of fuel cell systems. The use of a solid electrolyte eliminates most corrosion and liquid electrolyte management problems, and the high operating temperatures facilitate rapid electrode kinetics without the need for expensive noble metal electrocatalysts. Moreover the high quality heat produced is suitable for a variety of cogeneration applications. The principal disadvantage of ceramic fuel cells has been the complicated and relatively expensive processing procedures that are required to fabricate the tubular solid oxide fuel cell (SOFC) configuration favoured by Westinghouse. However recent developments in planar configuration technology have overcome many of these disadvantages. Moreover the introduction of metallic bipolar plates now allows ceramic fuel cells to be designed that can operate over a wide range of temperatures (450–950 °C). Many of these features have been discussed in a recent review by Minh [1], and so the present contribution will emphasise how the relative magnitude of oxygen ion and electronic conductivity can be manipulated to optimise the development of ceramic fuel cells operating at intermediate temperatures.

0378-7753/94/$07.00
SSDI 0378-7753(93)01789-K

In addition correlations between oxygen ion vacancy concentrations, chemical stability and thermal expansion coefficients in mixed conducting electrode components will also be discussed.

1.2. Performance parameters of SOFC stacks

At elevated temperatures the *I–V* characteristics of ceramic fuel cells are approximately linear; moreover the concentration overpotential contribution can usually be neglected. It follows that two principal parameters influence the magnitude of the oxygen flux value. The first is the area resistance, R_O (Ω cm^2), of the electrolyte component which may be expressed as L/σ, where L is the thickness (cm) of the electrolyte, and σ is the associated specific oxygen ion conductivity (S cm^{-1}). The second parameter involves the total interfacial resistance, R_A (Ω cm^2), associated with the relevant gas–solid reactions occurring at both electrodes. Provided the interfacial electrode kinetics are fast (i.e. overpotentials <50 mV) then each electrode resistance can be represented by the low field approximation of the Butler–Volmer equation

$$R_A = RT/j_O zF$$

where j_O is the appropriate exchange current density (A cm^{-2}).
From Ohm's Law, the overpotential (η) for a specific current density (j) is given by

$$\eta = (R_O + R_A)j$$

i.e.

$$j = \eta/(L/\sigma + RT/j_O zF)$$

If η is replaced by $(RT/4F) \ln pO_2'/pO_2''$, then the preceding equation is similar to one of the expressions derived by Liu [2] for mixed conducting ceramic membranes. If the interfacial resistance (R_A) can be ignored, then the expression becomes identical to the well known relationship

$$J = \frac{RT\sigma \ln pO_2'}{4F^2 L pO_2''} \text{ (mol O cm}^{-2}\text{ s}^{-1}\text{)}$$

derived by Wagner [3] sixty years ago for parabolic metal oxidation kinetics.

For the purpose of the present exercise it is important to realise that typical power densities for ceramic fuel cells operating at 950 °C approach 0.5 W cm^{-2} (0.7 V at 0.7 A cm^{-2}). As the Nernst potentials for 85% fuel conversion are around 0.9 V this power density performance implies total overpotential values at 0.7 A of approximately 0.2 V. The derived value for the individual cell area resistance is thus about 0.3 Ω cm^2. For subsequent discussions, therefore, it will be assumed that

$$R_O = R_A = 0.15\ \Omega\ \text{cm}^2$$

so that the corresponding values of L, σ and j_O can be determined.

2. Properties of SOFC components

2.1. Ionic and electronic conductivity

2.1.1. Electrolytes

It is appropriate to discuss specific electrical conductivity (σ: S cm^{-1}) in terms of the following expression:

$\sigma = nq\mu$

where n is the concentration (cm^{-3}) of relevant charge carriers, q is the charge (coulombs) on the carriers, and μ in the mobility ($cm^2\ s^{-1}\ V^{-1}$) of the carrier. For oxygen ion transport in SOFC components the charge carriers are usually oxygen vacancies (V_O), and Table 1 contains selected values for the relevant transport properties. High values for oxygen vacancy concentrations can be produced by aliovalent acceptor doping (e.g. $Zr_{0.9}Y_{0.1}O_{1.95}$), or by order–disorder processes in materials incorporating large concentrations of intrinsic structural anion vacancies, e.g. δ-Bi_2O_3, $Gd_2Zr_2O_7$. The maximum number of mobile anion vacancies available will be in the range 10^{21}–10^{22} cm^{-3}. If the specific ionic conductivity value is to exceed 10^{-1} S cm^{-1} then clearly the mobility term must be greater than 10^{-3} $cm^2\ s^{-1}\ V^{-1}$ according to the expression

$\sigma = 10^{-1} = nq\mu = (10^{21})(10^{-19})(10^{-3})$

Whilst it is possible to prepare oxygen ion conductors with specific conductivity values around 1 S cm^{-1} (e.g. δ-Bi_2O_3), it must be concluded that the associated values for both n and μ are approaching their upper limits. It is unlikely [4] that alternative oxygen ion electrolytes will be discovered with superior properties to those exhibited by ZrO_2- and CeO_2-based electrolyte materials, and it is important that design configurations focus on exploiting the behaviour of these two systems. As ceramic electrolytes are polycrystalline it is also necessary to consider the magnitude of grain boundary resistances. Fortunately by optimising powder purity and sintering procedures it is usually possible to reduce the grain boundary contribution to the total ceramic electrolyte resistance to around 20–30% [5].

Compared to liquids, a major feature of crystalline solids is that the mobility of electrons in the solid is usually many orders of magnitude greater than the mobility of ions (Table 1). For operation as an electrolyte it is essential that the ionic transference number ($t_{ion} = \sigma_{ion}/\sigma_T$) should be greater than 99%. There is clearly a requirement, therefore, for the concentration of electrons to be very small ($< 10^{-15}$ cm^{-3}). Unfortunately the level of electronic and hole conductivity is dependent upon oxygen partial pressure and temperature [6] due to reactions such as

$\frac{1}{2}O_2 + V_O^{\cdot\cdot} \longrightarrow O_O^x + 2h$: $\quad \sigma_h \propto pO_2^{1/4}$

$O_O^x \longrightarrow \frac{1}{2}O_2 + V_O^{\cdot\cdot} + 2e^-$: $\quad \sigma_e \propto pO_2^{-1/4}$

where $V_O^{\cdot\cdot}$ is the oxygen vacancy concentration, O_O^x is that of lattice oxygen, and h represents positive holes.

TABLE 1

Transport data for selected electrolyte and cathode materials at 1000 K

	$Zr_{0.9}Y_{0.1}O_{1.95}$		$Ce_{0.9}Y_{0.1}O_{1.95}$		$La_{0.6}Ca_{0.4}Co_{0.8}Fe_{0.2}O_{3-x}$	
	$V_O^{\cdot\cdot}$	e^a	$V_O^{\cdot\cdot}$	e^a	$V_O^{\cdot\cdot}$	p^b
σ (S cm^{-1})	1.5×10^{-2}	1.2×10^{-9}	6.3×10^{-2}	3.5×10^{-1}	9×10^{-3}	3×10^{-2}
μ ($cm^2\ V^{-1}\ s^{-1}$)	4.3×10^{-6}	9.8×10^{-3}	4.9×10^{-5}	6.8×10^{-4}	9.3×10^{-6}	5×10^{-2}
n (cm^{-3})	1.0×10^{22}	7.6×10^{11}	4×10^{21}	3.2×10^{21}	3×10^{21}	3.7×10^{22}

[a]Values calculated for $pO_2 = 10^{-20}$ bar (anodic: reducing conditions).
[b]Values calculated for $pO_2 = 1$ bar (cathodic: oxidising conditions).

At any particular temperature, therefore, there exists a range of oxygen partial pressures over which the ionic transference number is greater than 99% thus providing an ionic domain for application as a solid electrolyte. Ionic domains for $Zr_{0.9}Y_{0.1}O_{1.95}$ and $Ce_{0.9}Gd_{0.1}O_{1.95}$ are depicted in Fig. 1(a) and 1(b) at selected temperatures together with an indication of the associated ranges of oxygen partial pressures for typical fuel cell operation. Clearly the ionic domain for $Zr_{0.9}Y_{0.1}O_{1.95}$ allows its use as an electrolyte at both 950 and 650 °C. In contrast, the electronic conductivity exhibited by $Ce_{0.9}Gd_{0.1}O_{1.95}$ is too high at 800 °C under anodic conditions. However the ionic domain exhibited by $Ce_{0.9}Gd_{0.1}O_{1.95}$ is wider at 500 °C and so this material can be considered for use in direct methanol fuel cells (Section 4.1) operating at intermediate temperatures.

2.1.2. Cathodes

Although high electron mobilities can be a problem for oxide electrolytes, they are exploited in electrode materials. As will be discussed in the next section the kinetics of electrocatalytic reduction of oxygen are enhanced by the presence of both electronic and ionic conduction [4]. Evidence for this is provided by acceptor doped cobaltites

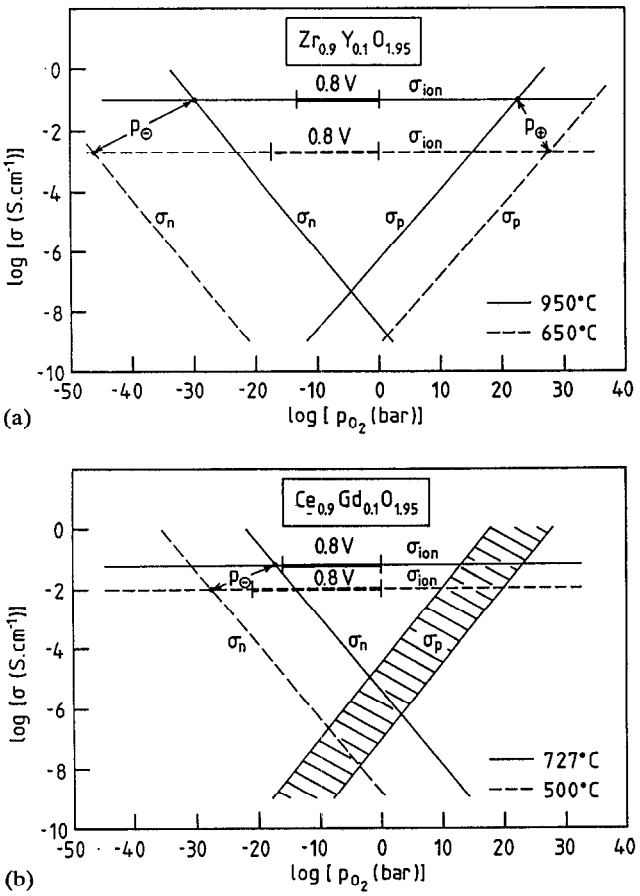

Fig. 1. Ionic and electronic conductivities as a function of oxygen partial pressure with indications of electrolytic domain and typical range of fuel cell operation: (a) $Zr_{0.9}Y_{0.1}O_{1.95}$; (b) $Ce_{0.9}Y_{0.1}O_{1.95}$.

such as $LaCo_{0.8}Fe_{0.2}O_{3-\delta}$ which exhibit high values for both electronic and ionic conductivities (Table 1). The associated high oxygen surface exchange coefficient ($\sim 10^{-5}$ cm s^{-1}) ensures very low oxygen reduction overpotentials [7]. In contrast the overpotentials associated with the manganites such as $La_{0.7}Sr_{0.3}MnO_3$ are much larger due to smaller values for the ionic conductivity and surface exchange coefficient.

A significant advantage of cathodes exhibiting mixed conductivity is that the requirement for optimising the three phase contact region is relaxed as the Faradaic reaction can occur over an extended region. Indeed providing the ionic conductivity is high enough then thin dense impermeable cathodes can be fabricated. Experiments at Imperial College have shown that thin (~ 1 μm) dense cathodes of $La_{0.6}Ca_{0.4}Co_{0.2}Fe_{0.8}O_3$ give lower electrode resistances at 800 °C than porous electrodes of the same materials. Similar results have been reported by Chen *et al.* [8]. The concept of using mixed ionic and electronic conductors for improved electrode performance is not new and has been proposed by many authors over the past thirty years [9–12]. However it has proved difficult to separate the relative contributions of surface kinetics, ionic and electronic conductivity. During the past ten years Steele and co-workers [13, 14] have developed a technique that involves $^{18}O/^{16}O$ isotopic exchange followed by determination of the ^{18}O diffusion profile in the solid by dynamic SIMS. This isotopic exchange/diffusion profile (IEDP) technique allows unambiguous derivation of both the oxygen surface exchange coefficient (k, cm s^{-1}) and oxygen surface self-diffusion coefficient (D^*, cm^2 s^{-1}). An example of these measurements is provided in Fig. 2 for $La_{0.6}Ca_{0.4}Co_{0.8}Fe_{0.2}O_{3-\delta}$. The oxygen self-diffusion coefficient (D^*) values can be used to calculate oxygen ion conductivity values via the Nernst–Einstein equation

$$\sigma/D^* = nq^2/kT$$

It is difficult to obtain ionic conductivity data in mixed conducting oxides by other methods although measurements involving electronic blocking electrodes have been attempted [15].

2.2. Oxygen surface exchange kinetics

The introductory section emphasised that low electrode overpotentials require high exchange current density values. Isotopic surface exchange (k) values determined by the IEDP technique provide data for the reaction

$$\tfrac{1}{2}O_2 + 2e^- + V_O^{\cdot\cdot} \longrightarrow O_O^x$$

and are directly related to the exchange current density (j_O) by the following expressions

molar surface exchange flux = J mol cm^{-2} s^{-1} $= j_O/zF = kV_M$

where V_M is the molar volume oxygen in the solid

i.e. $j_O = kV_M zF$

The accompanying Fig. 3 can be assembled from available data and it is immediately apparent that k and j_O values can vary by many orders of magnitude. The addition of Pt dispersed on the surface of $Zr_{0.9}Y_{0.1}O_{1.95}$ electrolytes increases values for k (and j_O) by about three orders of magnitude as Pt acts as a catalyst for the dissociative adsorption of oxygen molecules. However the k values for the Pt coated $Zr_{0.9}Y_{0.1}O_{1.95}$ electrolyte surfaces are below those obtained for uncoated $Ce_{0.9}Y_{0.1}O_{1.95}$ and $Bi_{0.8}Er_{0.2}O_3$ electrolytes. The surface of these electrolytes is catalytically active and indeed the addition of noble metal electrodes does not improve the k value. Electrochemical

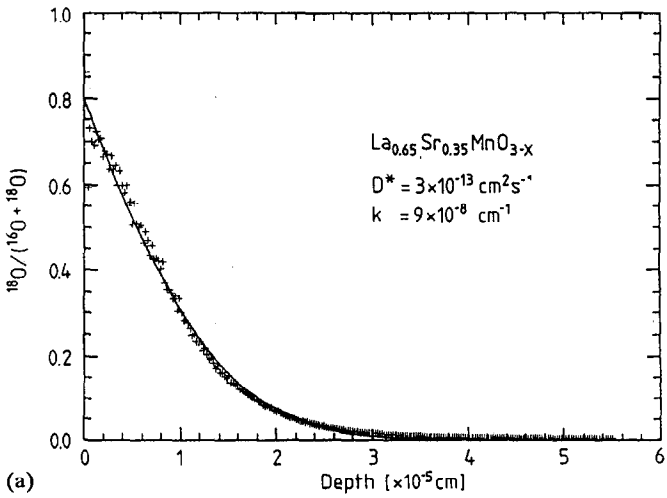

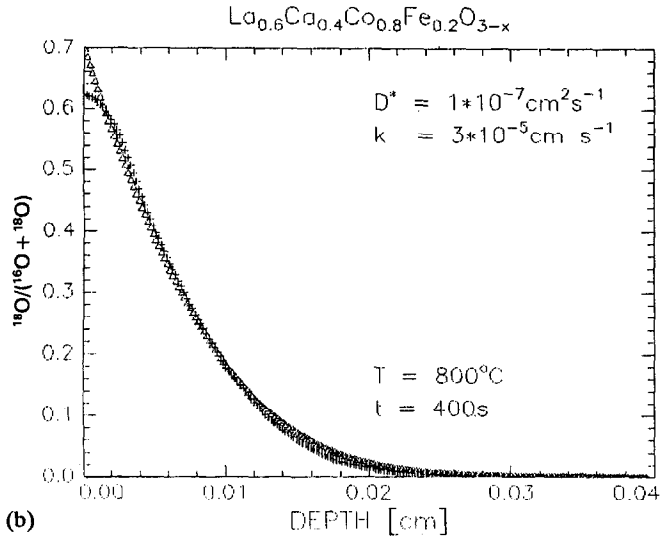

Fig. 2. (a) $^{18}O/^{16}O$ isotopic diffusion profile in $La_{0.65}Sr_{0.35}MnO_{3-x}$ for an anneal at 900 °C for 270 s; (b) $^{18}O/^{16}O$ isotropic diffusion profiles in $La_{0.16}Ca_{0.4}Co_{0.8}Fe_{0.2}O_{3-x}$.

measurements [16] on $Bi_{0.8}Er_{0.2}O_3$ have confirmed that j_O is independent of the type of noble metal used as electrode and directly related to k values obtained by isotopic exchange measurements on the uncoated ceramic electrolyte.

Attention is drawn to the surface exchange coefficient values in Fig. 2 for the perovskites $La_{0.65}Sr_{0.35}MnO_3$ (LMO) and $La_{0.6}Sr_{0.4}Co_{0.8}Fe_{0.2}O_3$. The values differ by two orders magnitude. Moreover the oxygen self diffusion coefficients (D^*) differ by six orders of magnitude [14]. When LMO is dispersed on $Zr_{0.9}Y_{0.1}O_{1.95}$ as a porous electrode and the three-phase contact regions optimised, it can then function as a satisfactory cathode material at 950 °C, but the exchange current density value is too low at 800 °C. However the combination of high k and D values for the cobaltite

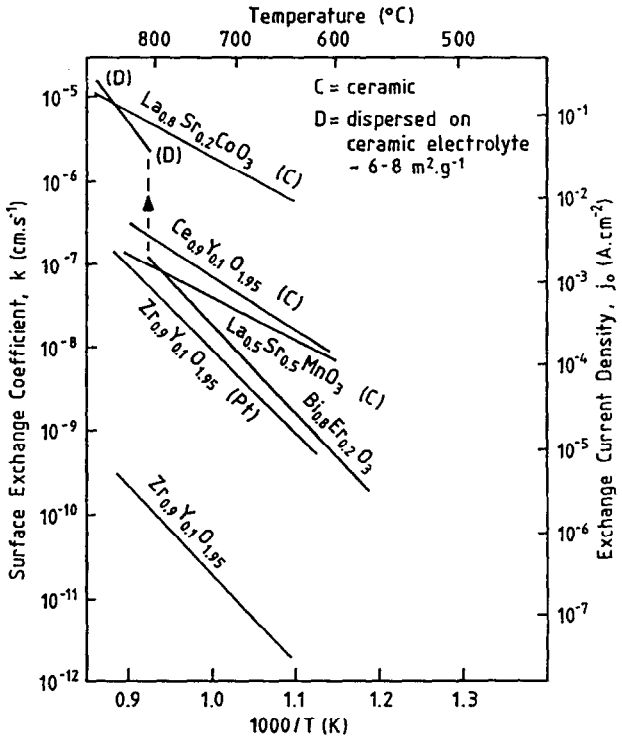

Fig. 3. Compilation of surface exchange coefficient values for selected oxides as a function of reciprocal temperature. B, Ceramic; D, dispersed on ceramic electrolyte about 6–8 $m^2\ g^{-1}$.

allow this material to be used as a very effective cathode at 800 °C provided that high resistance interfacial reaction products can be avoided, and that thermal expansion coefficient differences can be minimised. As already mentioned, it is possible to use thin impermeable cobaltite cathodes as the mixed conduction properties of this material relax the requirement for three-phase contact boundaries. The intrinsic conductivity and electrocatalytic properties of cobaltite perovskites make them very attractive candidates for SOFC cathodes and so their compatibility with ZrO_2 and CeO_2 ceramic electrolytes are considered in the following sections.

2.3. Thermal expansion behaviour of perovskite electrodes

Thermal expansion coefficients (*TEC*) reflect the vibrational amplitude of the constituent atoms (ions) which in turn is a measure of the pairwise interaction bonding energy. The introduction of oxygen vacancies, for example, in an oxide perovskite increases the unit cell dimensions as the ions relax somewhat from their normal lattice positions. The slope of the equilibrium potential energy/distance curve becomes less steep which allows larger vibration amplitudes for the remaining ions, and higher *TEC* values.

A conflict therefore arises between the need for a large concentration of oxygen ion vacancies to facilitate rapid oxygen ion mass transport, and thermal expansion coefficients matched to the appropriate ceramic electrolyte. Thermal expansion data

TABLE 2

Thermal expansion coefficient values for selected perovskite compositions

Composition	Thermal expansion coefficient (ppm K^{-1})	$V_O^{\cdot\cdot}$ concentration
$La_{0.45}Ca_{0.45}MnO_{3-x}$	11.7	I
$La_{0.84}Sr_{0.16}MnO_{3-x}$	11.9	N
$La_{0.8}Sr_{0.2}FeO_{3-x}$	12.0	C
$La_{0.5}Sr_{0.5}MnO_{3-x}$	13.2	R
		E
$La_{0.8}Sr_{0.2}Co_{0.2}Mn_{0.8}O_{3-x}$	14.2	A
$La_{0.5}Sr_{0.5}Co_{0.2}Mn_{0.8}O_{3-x}$	14.5	S
$La_{0.8}Sr_{0.2}Co_{0.2}Fe_{0.2}O_{3-x}$	15.0	I
		N
$La_{0.8}Sr_{0.2}CoO_{3-x}$	20.0	G
$La_{0.5}Sr_{0.5}CoO_{3-x}$	23.0	

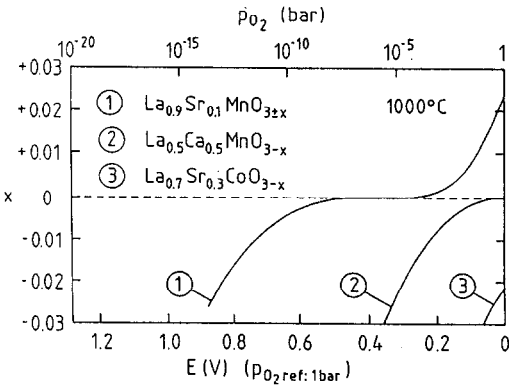

Fig. 4. Composition oxygen partial pressure isotherms for $La_{0.65}Sr_{0.35}MnO_{3-x}$, $La_{0.5}Ca_{0.5}MnO_{3-x}$ and $La_{0.7}Sr_{0.3}CoO_{3-x}$.

for selected SOFC components are given in Table 2. The different *TEC* values for the various perovskite materials can be correlated with the concentration of anion vacancies as indicated in the departures from ABO_3 stoichiometry shown in the composition oxygen partial pressure isotherms depicted in Fig. 4.

Depending upon the design configuration and operation it appears possible to tolerate a thermal expansion mismatch of about 10%. For $Zr_{0.9}Y_{0.1}O_{1.95}$ electrolytes this suggests an upper limit of *TEC* values around 12 ppm K^{-1}, so only manganite cathodes appear feasible with ZrO_2 electrolytes. In contrast, for $Ce_{0.9}Gd_{0.1}O_{1.95}$ electrolytes it should be possible to tolerate cathode expansivities up to 14 ppm K^{-1}. This higher value permits the use of selected cobaltite solid solutions, provided the cobalt content is not too high (Table 2).

2.4. Chemical compatibility: electrolytes/cathodes

Fabrication of ceramic cathode/electrolyte/anode (PEN) structures usually requires processing operations up to at least 1200 °C to ensure that the electrolyte is impermeable

TABLE 3

Cathode/electrolyte interfacial reactions

Cathode electrolyte interface	B cation	Reaction product
$La(Sr)BO_3/Zr_{0.9}Y_{0.1}O_{1.95}$	Fe^{3+}	$La_2Zr_2O_7$, $SrZrO_3$ (>1250 °C)
	Mn^{3+}	$La_2Zr_2O_7$, $SrZrO_3$ (>1150 °C)
	Co^{3+}	$La_2Zr_2O_7$, $SrZrO_3$ (>850 °C)
$La(Sr)BO_3/Ce_{0.9}Gd_{0.1}O_{1.95}$	Fe^{3+}	no reaction
	Mn^{3+}	no reaction
	Co^{3+}	$SrCeO_3$ > 1300 °C
$La(Ca)BO_3/Ce_{0.9}Gd_{0.1}O_{1.95}$	Co^{3+}	no reaction

and that good adherent electrode morphologies are developed. As SOFC operation is usually at lower temperatures (750–950 °C), the fabrication procedure is most demanding as to chemical stability.

Relative stabilities of oxide perovskite SOFC components in contact with ZrO_2 and CeO_2 electrolytes have been evaluated by Yokakawa *et al.* [17] and the principal conclusions of these investigations are summarized in Table 3.

Inspection of Table 3 shows that in contact with $Zr_{0.9}Y_{0.1}O_{1.95}$, all of the $La(Sr)BO_3$ perovskites incorporating Co^{3+}, Mn^{3+}, Fe^{3+} transition metal cations on the B site form the interfacial reaction products $La_2Zr_2O_7$ and $SrZrO_3$. However the temperature (T_R) at which significant reaction occurs can be correlated with the relative stability of the particular B^{3+} cation, namely, $Co^{3+}(T_R \sim 850\ °C) < Mn^{3+}(T_R \sim 1150\ °C) < Fe^{3+}(T_R \sim 1250\ °C)$. As the B^3 ion is reduced to the B^{2+} ion, anion vacancies are produced which reduces the stability of the ABO_3 perovskite structure.

All the ABO_3 perovskites are more stable in contact with $Ce_{0.9}Gd_{0.1}O_{1.25}$ electrolytes. The different radius ratios involved means that $La_2Ce_2O_7$ cannot be formed as a stable phase, and whilst $SrCeO_3$ can be produced it is less stable than $SrZrO_3$ and can only be formed at high temperatures (>1300 °C?). If the ABO_3 perovskite is doped with CaO instead of SrO then the stability is increased as $CaCeO_3$ is not stable. Moreover the use of CaO rather than SrO as dopant reduces the concentration of anion vacancies for a given composition which also ensures greater stability for the ABO_3 cathode.

Both chemical stability considerations and *TEC* values confirm that certain cobaltite compositions can be selected as cathodes for $Ce_{0.9}Gd_{0.1}O_3$ ceramic electrolytes.

3. Materials selection for SOFC operation at 800 °C

Operation at 800 °C would allow the use of conventional cheaper alloys for the balance of plant equipment such as heat exchangers, ducting, pumps, etc. Examination of Fig. 5 indicates that for $Zr_{0.9}Y_{0.01}O_{1.95}$ (ZYO), the largest value of L/σ <0.15 Ω cm^2 can only be attained if the electrolyte thickness is less than about 35 μm. This electrolyte thickness is comparable to that (~40 μm) used in the Westinghouse tubular technology, which employs a CVD/EVD processing route to deposit the electrolyte onto a porous $La_{0.8}Sr_{0.2}MnO_3$ cathode tube. Allied signal have also reported [18] the fabrication of thin (~5 μm) dense impermeable zirconia electrolytes on a porous Ni–ZrO_2 anode substrate by calendering techniques. Fabrication routes are thus available

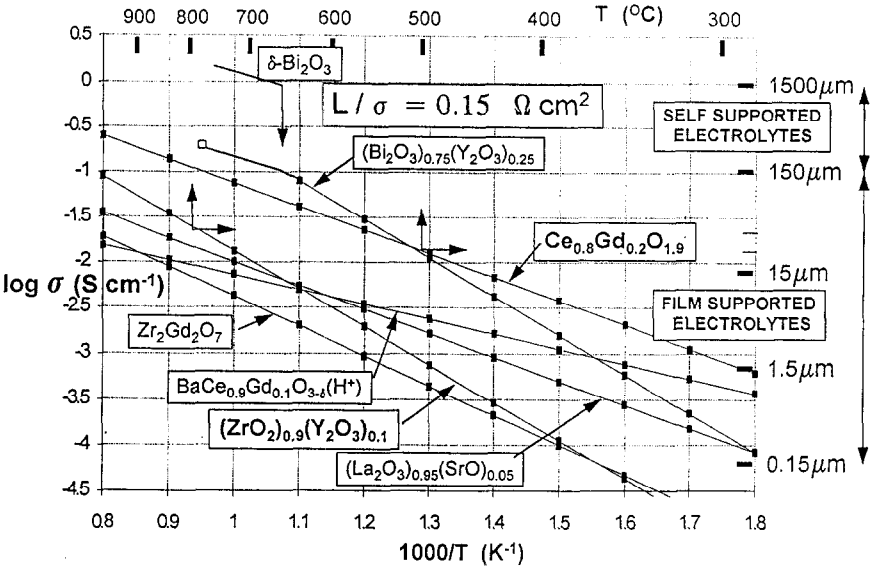

Fig. 5. Specific ionic conductivity values for selected oxide electrolytes as a function of reciprocal temperature.

to prepare dense zirconia electrolytes of the required thickness but unfortunately $La_{(1-x)})Sr_xMnO_3$ (LSM) cathode compositions exhibit relatively large electrode resistances ($> 0.15\ \Omega\ cm^2$) at 800 °C (Section 2.2). Furthermore it has not been demonstrated that the planar Ni–ZrO_2 substrate supported zirconia electrolyte structure has sufficient mechanical integrity when subjected to mechanical and thermal stresses. It would be desirable to replace LSM cathodes by LSCM or LSCF compositions (Section 2.2) but the cobalt-containing electrodes are likely to react with the zirconia electrolyte during the fabrication stage (Section 2.4). An obvious solution would be to use a thicker ceria-based electrolyte to support the thin zirconia electrolyte. This would allow the use of LSCM or LSCF cathode compositions as the ceria electrolyte also acts as a buffer for thick film ZYO in contact with the porous Ni–ZrO_2 anode. Inspection of Fig. 5 reveals that a 145 μm thick $Ce_{0.9}Gd_{0.1}O_{1.95}$ electrolyte substrate could support a 10 μm thick $Zr_{0.9}Y_{0.1}O_{1.95}$ electrolyte layer and still satisfy the target electrolyte area resistance value of 0.15 $\Omega\ cm^2$. Obviously other combinations of composite electrolyte thicknesses are possible. Some of these have been reported in the literature.

An important conclusion from this analysis is that it is already possible to select materials from available compositions that should allow individual PEN assemblies to operate at 800 °C at power densities approaching 0.5 W cm^{-2}. A typical arrangement could be:

$$\oplus\ LSCF/Ce_{0.9}Gd_{0.1}O_{1.95}(145\ \mu m),\ Zr_{0.9}Y_{0.1}O_{1.95}/Ni\text{–}ZrO_2\ \ominus$$

This configuration assumes that the Ni–ZrO_2 anode can successfully operate in an internal reforming mode at 800 °C. There is some evidence to suggest that this is possible and further comments on this topic are made in Section 4.2.

Assembly of the individual PEN structures into a stack also requires the selection of an appropriate bipolar plate or interconnect material. Ceramic materials based on doped $LaCrO_3$ compositions do not possess sufficient electronic conductivity at 800 °C to allow 0.5 W cm^{-2} power densities to be achieved. Moreover, the ceramic

interconnects are relatively expensive due to high fabrication costs. In contrast, the metallic bipolar plate developed by Siemens [19] offers an excellent solution, and operation at 800 °C will reduce any degradation problems encounted when using this bipolar plate material at 950 °C. The superior thermal conductivity exhibited by metallic bipolar plates also facilitates stack thermal management procedures. It should also be noted that formation of the protective oxide coating on the metallic bipolar plate also provides an interesting example of the optimisation of the associated electronic and ionic conductivities. The electronic conductivity of the oxide coating must be sufficiently high to ensure low interfacial contact resistances between the anode and cathode of adjoining cells. At the same time, the ionic fluxes should be as low as possible to ensure that the coating thickness increases only slowly over extended periods.

It may be concluded, therefore, that stack materials are available for 800 °C operation, and performance data are urgently required on scaled-up multi-kilowatt units under these conditions.

4. Future developments

4.1. Operation at 500 °C

In Section 2.1.1 attention was drawn to the relatively wide ionic domain for $Ce_{0.9}Gd_{0.1}O_{1.95}$ (CGO) electrolytes at 500 °C. The range and position of this ionic domain (Fig. 1(b)) allows this material to be considered for use in fuel cells operating around 500 °C. Provided that the CGO electrolyte thickness does not exceed 20 μm, the area resistance should be lower than the target value 0.15 Ω cm^2 (see Fig. 5). Since processing technology already allows the fabrication of supported electrolyte structures thinner than 20 μm, the CGO electrolyte component should be adequate for 500 °C operation. A metallic bipolar plate can also be selected, so attention needs to be focussed on the performance of appropriate cathode and anode materials. If electrodes can be developed with satisfactory performance, then ceramic fuel cells operating around 500 °C should be viable systems for transport applications using methanol fuel. A design for use as a 'range-extender' in a hybrid battery/fuel cell electric vehicle operation in the temperature range 400–500 °C should be feasible, as there would be sufficient time for the ceramic fuel cell to attain the required operating temperature. Obviously the structural integrity of the PEN assembly requires evaluation when subjected to the thermal stresses associated with rapid heating/cooling cycles, and to fatigue degradation associated with vibration. However design constraints are somewhat more relaxed at lower temperatures, so that PEN structures can be maintained in compression using compliant gasket materials.

The successful demonstration of ceramic fuel cells operating at 500 °C will undoubtedly arouse widespread interest, and provide a significant impetus to the development of electric vehicles.

4.2. Protonic conductivity and anode development

The present contribution has focussed on the properties and performance of ceramic electrolytes and cathodes, principally because our understanding of the behaviour of these components is presently more advanced than is the case for anodes. However, over the past ten years there has been an increasing recognition that all acceptor doped oxides can dissolve water according to the reaction:

$$H_2O + V_O^{\cdot\cdot} \longrightarrow O_O^x + 2H_i$$

where H_i represents dissolved protons.

Indeed for compositions incorporating basic oxides such as BaO it is possible to dissolve significant quantities of water. The perovskite material $BaCe_{0.9}Gd_{0.1}O_{3-\delta}$ for example, is a predominant protonic conductor under selected temperature and pH_2O regimes [20, 21]. Many more examples have been reported in the literature, and during our IEDP measurements at Imperial College we always detect a significant OH^- signal in the dynamic SIMS instrument. The presence of protons in the ceramic oxide appears to facilitate oxygen mass transport as the OH^- species has a smaller volume than O^{2-}. This may be the explanation for the observation of significant rates of oxygen transport at room temperature in compounds such as $YBa_2Cu_3O_{7-x}$ and $Sr_2Fe_2O_{5-x}$ [22].

Investigations at Imperial College [23] suggest that the catalytic activity of acceptor doped oxides for the complete oxidation of methane to carbon dioxide and water at intermediate temperatures is influenced by the presence of protons in the oxide lattice. Experiments are now underway involving $^2D/^1H$ exchange experiments and SIMS to determine whether the catalytic activity for methane oxidation can be correlated with $^2D/^1H$ surface exchange coefficients. These investigations are obviously stimulated by the success in explaining the relative rates for the cathodic reduction of oxygen in terms of $^{18}O/^{16}O$ surface exchange coefficient (Section 2.2).

If it can be demonstrated that protons and oxygen ions have a role in the catalytic oxidation of methane then it is likely that alternative anodes to $Ni–ZrO_2$ can be developed which will reduce the steam/methane ratio that is currently required for internal reforming in SOFC stacks.

4.3. Complementary technology: ceramic electrochemical reactors

A major advantage of ceramic fuel cells is that they represent only one example of a generic ceramic electrochemical reactor (CER) technology. CER systems can also be used to supply oxygen (e.g. separation of oxygen from air), or to produce chemicals (e.g. propane → acrolein) using partial oxidation reactions. The development of intermediate temperature ceramic fuel cells is stimulating these other applications and it should be noted that an oxygen generator supplying 20 litres of O_2 per min has a stack size comparable to a 20 kW fuel cell. These alternative market opportunities for CER technology are leading to a recognition that the investment risk for ceramic fuel cells may be lower than for other fuel cell systems. Accordingly more companies are now starting programmes involving CER technology which will also benefit the development of intermediate temperature fuel cells.

5. Conclusions

The mobilities of oxygen ion vacancies are orders of magnitude lower than the mobilities of electronic charge carriers, so for electrolyte applications the concentration of electronic charge carriers must be minimised and anion vacancy concentration maximised. An examination of the parameters involved suggests that it is unlikely that novel oxygen ion electrolytes will be produced that exhibit significantly better properties than ceria or zirconia fluorite materials.

For electrodes the restriction on the concentration of electrons is relaxed, and a wider range of structure types can be considered. However additional features such as thermal expansion and chemical stability with the adjoining electrolyte must be evaluated. In practice, therefore, only a limited number of materials satisfy the selection

criteria, and for 800 °C operation the solid solutions $La_{1-x}(Sr/Ca)_xCo_{1-y}(Fe/Mn)_yO_{3-\delta}$ appear to be the most promising materials in contact with ceria-based substrate/buffer electrolyte layers, since they can exhibit very high oxygen surface exchange coefficient values.

Because materials are now available for 800 °C operation, research effort is being switched to investigate direct methanol ceramic fuel cells operating around 450–500 °C using ceria-based electrolytes.

Novel cathode and anode compositions are needed, but the lower temperature operation fortunately allows a greater range of oxides to be considered for electrodes. It will also be important to generate information as soon as possible on the structural stability of these combinations for applications in electric vehicles.

Finally it is likely that the role of protons in oxides will receive more attention in the future, particularly in the development of alternative anodes.

Acknowledgements

The author thanks present colleagues in the Centre for Technical Ceramics for useful discussions and for providing experimental data. Financial support from the Science and Engineering Council, the Commission of the European Communities, and the Club of Industrial Affiliates for the Development of Ceramic Electrochemical Reactors is also gratefully acknowledged.

References

1 N.Q. Minh, *J. Am. Ceram. Soc., 76* (1993) 563.
2 M. Liu, in T.A. Ramanaryan and H.L. Tuller (eds.), *Ionic and Mixed Conducting Ceramics,* Vol. 91-12, The Electrochemical Society, Inc., Pennington, NJ, 1991, p. 95.
3 C. Wagner, *Z. Phys. Chem., Abt. B, 21* (1993) 25.
4 B.C.H. Steele, *Mater. Sci. Eng., B13* (1992) 25.
5 B.C.H. Steele, in S.P.S. Badwal, M.J. Bannister and R.H.J. Hannink (eds.), *Science and Technology of Zirconia V,* Technomic Publishing Company, Inc., Lancaster, PA, USA, 1993, p. 713.
6 B.C.H. Steele and C.B. Alcock, *Trans. A.I.M.E., 233* (1965) 1359.
7 O. Yamamoto, Y. Takeda, R. Kanno and M. Noda, *Solid State Ionics, 22* (1987) 241.
8 C.C. Chen, M.M. Nasrallah and H.U. Anderson, in S.C. Singhal and H.Iwahara (eds.), *Proc. 3rd Int. Symp. Solid Oxide Fuel Cells,* Vol. 93-4, The Electrochemical Society, Inc., Pennington, NJ, 1993, p. 598.
9 H.H. Mobius and B. Rohland, *US Patent No. 3 377 203* (Apr. 9, 1968).
10 T. Takahashi, in J. Hladik (ed.), *Physics of Electrolytes,* Vol. 2, Academic Press, New York, 1972, p. 1034.
11 B.C.H. Steele, in W. Van Gool (ed.), *Fast Ion Mobility in Solids,* North-Holland, Amsterdam, 1973, p. 103.
12 P. Van Den Berghe and H. Tannenberger, *US Patent No. 4 130 693* (Dec. 19, 1978).
13 J.A. Kilner, L. Ilkov and B.C.H. Steele, *Solid State Ionics, 12* (1984) 89.
14 S. Carter, A. Selcuk, R.J. Chater, J. Kajda, J.A. Kilner and B.C.H. Steele, *Solid State Ionics, 53/56* (1992) 597.
15 W.L. Worrell, *Solid State Ionics, 52* (1992) 147.
16 B.C.H. Steele, J.A. Kilner, P.F. Dennis, A. McHale, M. Van Hemert and A.J. Burggraaf, *Solid State Ionics, 18/19* (1986) 1038.
17 H. Yokakawa, N. Sakai, T. Kawada and M. Dokiya, *J. Solid State Chem., 94* (1991) 106.
18 N.Q. Minh, T.R. Armstrong, J.R. Esopa, J.V. Guiheen, C.R. Horne and J.J. Van Ackeren, in S.C. Singhal and H. Iwahara (eds.), *Proc. 3rd Int. Symp. Solid Oxide Fuel Cells,* Vol. 93-4, The Electrochemical Society, Inc., Pennington, NJ, 1993, p. 801.

19 E. Ivers-Tiffee, W. Wersing, M. Schiessl and H. Greiner, *Ber. Bunsenges. Phys. Chem., 94* (1990) 978.
20 H. Uchida, N. Maeda and H. Iwahara, *J. Appl. Electrochem., 12* (1982) 645.
21 N. Bonanos, *Solid State Ionics, 53/56* (1992) 967.
22 A. Wattiaux, L. Fournes, A. Demourgues, N. Bernaben, J.C. Grenier and M. Pouchard, *Solid State Commun., 77* (1991) 489.
23 P.H. Middleton, H.J. Steiner, G.M. Christie, R. Baker, I.S. Metcalfe and B.C.H. Steele, in S.C. Singhal and H. Iwahara (eds.), *Proc. 3rd Int. Symp. Solid Oxide Fuel Cells,* Vol. 93-4, The Electrochemical Society, Inc., Pennington, NJ, 1993, p. 542.